Second Order Sliding Mode Control of Oscillating Water Column Wave Energy Converters for Power Improvement

Daniel T. Gaebele, *Student Member, IEEE*, Mario E. Magaña, *Senior Member, IEEE*, Ted K. A. Brekken, *Senior Member, IEEE*, João C. C. Henriques, Ana A. D. Carrelhas, and Luís M. C. Gato

***Abstract*—Ocean wave energy is a renewable energy which remains too costly for large-scale electricity generation. The oscillating water column (OWC) wave energy converter (WEC) is a promising device-type with a rectifying air turbine and generator which convert alternating airflow induced by the water motion into kinetic energy then into electric energy. Applying control at each stage of energy conversion could increase the electric energy output of the device. As researchers overcome the modeling challenges of OWC, such as the nonlinearities due to air compressibility and power take-off (PTO) dynamics, we can integrate specific control algorithms to test their ability to improve the efficiency of the OWC. Herein, we present a state-space model of an array of OWC WECs restricted to heave motion with nonlinear PTO dynamics. We apply second-order sliding mode control (SMC) which commands a smooth torque signal to a direct-drive generator to maintain a reference turbine angular velocity. Because the algorithm can yield high turbine torques, we investigate a simple feed-forward relation for the control of a valve to limit the turbine airflow and discard mechanical power. We find that implementing the SMC algorithm and valve control can improve electric energy conversion most effectively in less energetic sea states.**

***Index Terms*—Wave energy conversion, oscillating water column, sliding mode control, biradial turbine.**

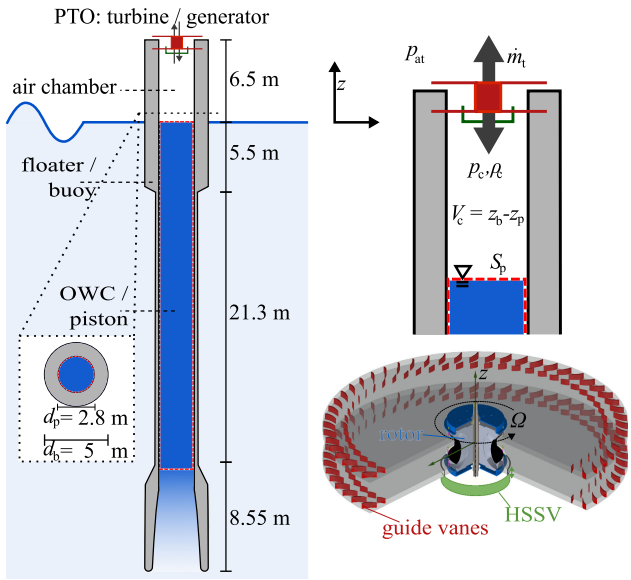

Fig. 1. Conceptual sketch of a floating OWC equipped with one turbine on the left. On the right a close up of the air chamber and the biradial turbine.

I. Introduction

CONTROLS research for ocean wave energy converters began concurrently with the first fundamental research in the field in the 70s [1]. In the following years, the efforts remained mostly academic due to the theoretical complexity of the hydrodynamic interactions between waves and oscillating bodies [2]. With improving hardware, wave energy research activity has increased over the last two decades [3]. One of the reasons why no commercial application is yet fully realized is the high cost compared to other renewable energy sources [4]. The largely random variability of energy flux over time is one disadvantage of wave power. However, with intelligent control approaches, this disadvantage can be overcome [5]. Intelligent control may also reduce the power fluctuations from WEC arrays, which in turn reduce the overall maintenance cost [6].

Our recent and current research [7] addresses the control of arrays of floating oscillating water column (OWC) wave energy converters (WECs) pictured in Fig. 1. This semi-submerged, hollow, off-shore device is open to the ocean at the bottom and traps air inside a chamber separated by an air turbine from the atmosphere (illustrated in Fig. 1). Since OWCs have few moving parts and the power take-off (PTO) has no water contact, they are considered one of the least complicated WECs [8]. Suitable air turbines for the PTO are self-rectifying, meaning they have unidirectional rotation even though the air flow is

Manuscript received April 24, 2020; revised August 13, 2020 and September 29, 2020; accepted October 28, 2020. Date of publication November 3, 2020; date of current version March 22, 2021. This work was completed in part by the Oregon State University team which was sponsored by the National Science Foundation, USA (under awards 1711859) and in part completed by the IDMEC/IST team which was funded by the Portuguese Foundation for Science and Technology (FCT) through IDMEC, under LAETA Project UIDB/50022/2020. Paper no. TSTE-00433-2020. *(Corresponding author: Daniel T. Gaebele.)*

Daniel T. Gaebele, Mario E. Magaña, and Ted K. A. Brekken are with the Department of Electrical and Computer Engineering, Oregon State University, Corvallis, OR 97331 USA (e-mail: gaebeled@oregonstate.edu; magana@eecs.oregonstate.edu; brekken@eecs.oregonstate.edu).

João C. C. Henriques, Ana A. D. Carrelhas, and Luís M. C. Gato are with the IDMEC, Instituto Superior Técnico, Universidade de Lisboa, 1049-001 Lisboa, Portugal (e-mail: joaochenriques@tecnico.ulisboa.pt; ana.carrelhas@tecnico.ulisboa.pt; luis.gato@tecnico.ulisboa.pt).

Color versions of one or more of the figures in this article are available online at https://ieeexplore.ieee.org.

Digital Object Identifier 10.1109/TSTE.2020.3035501

bidirectional due to the oscillating motion of the waves. In terms of performance, the biradial turbine is a better choice due to the higher peak efficiency and smooth decrease of efficiency for large flow rate coefficients, in comparison with the well-known Wells turbine[8]. Therefore, we select the biradial turbine for this work along with the dynamic model from [9]. We present the dynamics as a function of the position of a high speed stop valve (HSSV), installed in front of the turbine. The biradial turbine is suitable to directly attach a generator, removing the need for an expensive and less-reliable gearbox. As in [10], we use the physical parameters of a specific squirrel cage induction machine to implement a generator, namely the SIEMENS IEC low-voltage electrical generator model 1LE1603-2AB53-4GB4-Z, to produce electricity from the ocean waves [11], [12]. The generator, driven by the turbine, has to oppose the acting torque quantified by the control algorithm.

The approach we use in this paper is sliding mode control (SMC) due to its robustness and ability to handle uncertain nonlinear dynamics by applying a discontinuous control signal to force the system into a subset of the system's regular behaviour [13]. The discontinuities can result in the phenomenon called chattering, which is potentially harmful to the actuators. Therefore, it is common practice to smooth out the signal with, for example, a continuous approximation of the `signum` function. First-order SMC has been previously applied to fixed OWCs that are equipped with Wells turbines and double-fed induction generators (DFIG) [14], [15] as well as those equipped with synchronous AC generators attached to the biradial turbines [16]. A shortcoming of first-order SMC is that it will command any numerical value necessary to achieve the control goal without accounting for the physical limitations of the components, potentially leading to failure.

A remedy can be achieved using second-order SMC. The most popular second-order SMC in the renewable energy literature is the super-twisting algorithm (STW) after Levant [17]. For example the speed control of a doubly-fed induction generator (DFIG) [18] and a permanent magnet synchronous machine (PMSM) [19], both driven by wind turbines. Application in current turbines include the control of again a DFIG [20] and a doubly salient permanent generator [21]. Previous application of STW SMC in wave energy conversion has been conducted on a fixed OWC with an impulse turbine driving a PMSM [22] and as part of a comparison between different second-order SMCs applied to floating OWCs [23], which were originally proposed in the fundamental work on SMC [17], [24]. Commonly in those SMC applications maximum power point tracking schemes are used to calculate the reference angular velocity. However, in this work we investigate the performance with a constant reference speed, which is based on the averaged rotational speed for the current sea state, originating from a benchmark control law that maximizes the aerodynamic efficiency of the biradial turbine. The main requirements for the proposed controller are a smooth control signal and to respect the physical constraints of the used squirrel cage generator, i.e. the maximum applicable generator torque and the rated generator power. To do so, instead of using the STW SMC we apply a second-order SMC approach with a prescribed law of variance, which does not tend to overshoot after the control limit is reached [23], but this comes with the disadvantage of requiring more inputs to the algorithm. Maintaining the optimized rotational speed results in an efficient area of operation for both the turbine and especially the generator.

Since the SMC keeps the rotational speed higher than it would be in the uncontrolled case, the generator torque as soon as pressure is induced can also be higher. To address this drawback we implement a feed forward control to limit the turbine air flow with the HSSV based on the instantaneous turbine torque. We do so with the simplest form of a fuzzy logic control (FLC). FLC has been previously applied to WECs in [25]. We choose an FLC approach due to the fact that with FLC we can implement an intuitive operating mechanism [26] and, in case we want to build upon the FLC in future work, the nonlinear air chamber dynamics can be easily considered. Air flow control of fixed OWCs and the necessary sensors are addressed in [27].

The floating OWC buoy geometry used in this work is based on the data publicly available of the IDOM Marmok A-5 spar-buoy [28]. This buoy has been successfully deployed during three years at the BiMEP test site (Basque Country, Spain) within the H2020 OPERA Project (http://opera-h2020.eu/). The hydrodynamic model of the buoy is based on the linear wave theory and is described in [7]. The hydrodynamic coefficients were obtained using the boundary element method solver (ANSYS Aqwa) considering the hydrodynamic interactions between different WECs inside the array. Subsequently, we present the derivation of the control algorithms, namely, the sliding mode control for the generator torque and briefly the control for the position of the HSSV and a benchmark control law. We evaluate the power improvement capabilities of different control cases in varying wave climates and discuss further research.

II. Dynamic Model

In our prior work [7] we describe the dynamic equations of an array of N floating OWC WECs applied to the Marmok-A-5 type WEC equipped with an identical biradial turbine. This work highlights aspects important for the control design and restates the state space representation with the control design oriented notation we presented in [23]. The hydrodynamic model is based on the common assumption of small wave amplitudes and body motions compared to the wave lengths. Therefore, the linear water wave theory is applicable. An imaginary rigid piston will represent the internal free surface of the OWC since its diameter is much smaller than the wave lengths. This assumption enables us to apply oscillating body theory between the buoy and piston, called a two-body heaving system as in [1] and illustrated in Fig. 1. Throughout the paper, we will use the terms piston and OWC interchangeably. Our research focuses on the motion in heave direction because of the significance for power production of the floating OWC. We define a positive displacement $z(t)$ to be in upwards direction and $z(t) = 0$ at the calm ocean surface. The dynamics in $z(t)$ are contained in our state vector which we define for the array of N WECs and consequently $2N$ bodies,

$$\boldsymbol{x} = \begin{bmatrix} \boldsymbol{x}_z & \boldsymbol{x}_v & \boldsymbol{x}_{p^*} & \boldsymbol{x}_\Omega \end{bmatrix}^T. \tag{1}$$

Here $\boldsymbol{x}_z \in \mathbb{R}^{1\times 2N}$ denotes heave positions and $\boldsymbol{x}_v \in \mathbb{R}^{1\times 2N}$ denotes the heave velocities of the bodies $i \dots 2N$, thus

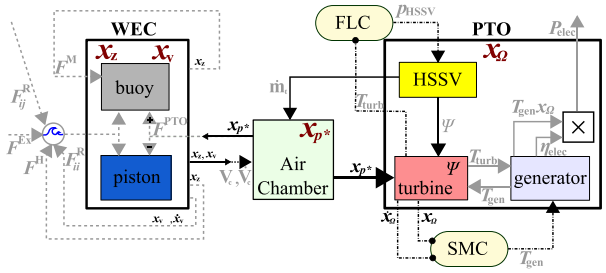

Fig. 2. Components of the floating OWC with the state variables, the acting forces and the signal used for the control algorithms.

$x_{z,i} = z_i = x_i$, $x_{v,i} = \dot{z}_i = x_{2N+i}$. There are two more quantities storing energy in the WEC system. First, the pressure in the air chamber is accounted for in the vector of the relative pressure difference $\boldsymbol{x}_{p^*} \in \mathbb{R}^{1\times N}$ of WEC $i \dots N$. Second, the rotational speeds of the turbine/generator sets are contained in the vector $\boldsymbol{x}_\Omega \in \mathbb{R}^{1\times N}$ of system $i \dots N$, respectively, therefore $x_{p^*,i} = p_i^* = x_{4N+i}$ and $x_{\Omega,i} = \Omega_i = x_{5N+i}$. Consequently, $\boldsymbol{x} \in \mathbb{R}^{1\times 6N}$. In Fig. 2 the state vectors are illustrated with the black font. Fig. 2 contains the acting forces in grey dotted and important quantities that are introduced in the derivation of the dynamic model described below.

A. Hydrodynamic Model

The Cummins equations for the considered two-body heaving system oscillating in heave in the ocean are given by,

$$m_\mathrm{b}\ddot{x}_{z,i}(t) = F_i^\mathrm{H}(t) + F_i^\mathrm{M}(t) + F_i^\mathrm{Ex}(t) + F_i^\mathrm{R}(t) + F_i^\mathrm{PTO}(t) \tag{2}$$

$$m_\mathrm{p}\ddot{x}_{z,i}(t) = F_i^\mathrm{H}(t) + F_i^\mathrm{Ex}(t) + F_i^\mathrm{R}(t) - F_i^\mathrm{PTO}(t). \tag{3}$$

Here m_b and m_p denote the mass of a buoy and piston, respectively. If the i^{th} body is a buoy equation (2) describes the dynamics and for a piston the dynamics are described by (3). The considered forces are,

- F^H The hydrostatic restoring force, adding heave position depending spring like effect, zero at equilibrium.
- F^M The mooring force due to mooring connection to the sea floor. No mooring is connected to the imaginary piston.
- F^Ex The excitation force accounts for all incident waves on the body.
- F^R The radiation force, including interactions with the motion of other bodies in the array. Results from solving the radiation problem.
- F^PTO The force due to the pressure change in the chamber induced by the turbine/generator dynamics. Acting in opposite direction for buoy and OWC.

Nonlinear viscous and other friction effects are neglected in our OWC WEC studies, since those viscous losses are reduced due to the vertically-cut ring torus shape of the buoy's bottom. However, the time-domain formulation of the equations of motion allows the practical correction to add those terms [1]. In Fig. 2 the diagonal arrow with label F_{ij}^R represents the radiation force due to oscillation of spatially distinct WECs inside the array. Furthermore, we will give a comprehensive presentation of the air chamber and the PTO dynamics because of the importance of $F_i^\mathrm{PTO}(t)$ for the nonlinear control design. To obtain the local wave-induced excitation force we superpose N_w wave components as in [9]

$$F_i^\mathrm{Ex}(t) = \sum_{k=1}^{N_\mathrm{w}} \Gamma_i(\omega_k,\theta) A_k \cos\left(\omega_k t + \phi_k + \Phi_i^\mathrm{Ex}(\omega_k,\theta)\right). \tag{4}$$

Here $\Gamma_i(\omega_k,\theta)$ and $\Phi_i^\mathrm{Ex}(\omega_k,\theta)$ denote the hydrodynamic excitation coefficient and the corresponding phase component, respectively. They will strongly vary for different WECs and array configurations, due to the diffraction problem of the incident wave fields, with wave frequency ω_k and incident wave angle θ. We use a Pierson-Moskowitz wave energy spectrum to compute the amplitude components A_k based on the significant wave height H_s and wave period T_p. Lastly, ϕ_k is the uniformly distributed random phase component, which yields an irregular wave.

The radiation problem yields more hydrodynamic coefficients which can be taken into account for in the time domain representation with the force

$$F_i^\mathrm{R}(t) = \underbrace{\sum_{j=1}^{2N} A_{ij}^\infty \ddot{x}_{z,j}(t)}_{F_i^{\mathrm{R},\infty}} - \underbrace{\sum_{j=1}^{2N} \int_0^t K_{ij}(t-\tau)\dot{x}_{z,j}(\tau)\mathrm{d}\tau}_{F_i^{\mathrm{R}'}}, \tag{5}$$

acting on body i due to body j. With the state space representation in mind, the radiation force is separated into two components. The first component $F_i^{\mathrm{R},\infty}$ explicitly depends on the acceleration $\ddot{x}_{z,j}$ and the second component $F_i^{\mathrm{R}'}$ explicitly depends on the velocity $\dot{x}_{z,j}$ of the j^{th} body. Here A_{ij}^∞ represents the constant added mass on body i due to motion of body j, as a result of the frequency dependent added mass $A_{ij}(\omega)$ evaluated at $\omega \to \infty$ as in Cummins formulation . The kernel function of the convolution integral in (5) incorporates the frequency dependent radiation damping coefficient $B_{ij}(\omega)$ into the radiation force component depending on the velocity, via the inverse Fourier transformation

$$K_{ij}(t) = \frac{2}{\pi}\int_0^\infty B_{ij}(\omega)\cos(\omega t)\mathrm{d}\omega \approx \sum_{k=1}^{N_{\mathrm{K},ij}} \alpha_{ij,k}\mathrm{e}^{\beta_{ij,k}t}. \tag{6}$$

Consequently, instead of using the two real, frequency dependent matrix functions $A(\omega)$ and $B(\omega)$ we use the time dependent matrix function $K(t)$ and the constant matrix A^∞ containing the same hydrodynamic information. This is known as the Kramers-Kronig relation in hydrodynamic radiation. The derivation using the principle of causality is described in [1] in detail. Instead of solving the convolution integral in (5) at every time step, we approximate it with a linear state space representations that shares the same impulse response. The approximation of $K_{ij}(t)$ is achieved by Prony's method with decaying exponentials, described by the Prony coefficients $\alpha_{ij,k}, \beta_{ij,k} \in \mathbb{C}$, for further details see [10] and [7].

The asynchronous oscillation of the buoy and the piston yields a varying pressure inside the air chamber $p_i(t)$ due to the relative motion. This chamber pressure relative to the atmospheric pressure $p_i(t) - p_\mathrm{at}$ acts as a force in opposite direction on the

buoy and piston [9], namely,

$$F_i^{\text{PTO}}(t) = \begin{cases} (p_i(t) - p_{\text{at}})\, S_{\text{p}}, & \text{for a buoy} \\ -(p_i(t) - p_{\text{at}})\, S_{\text{p}}, & \text{for a piston} \end{cases}. \tag{7}$$

The dynamics of the chamber pressure are influenced by the spatial states x_z, $\dot{x}_z$ and significantly by the PTO. The PTO defines the air flow in or out of the chamber through the turbine generator set and the high speed stop valve.

B. Power Take-Off Model

The air compressibility introduces nonlinearities to the OWC dynamics which are modeled in detail in [9] together with the dynamics of the biradial turbine. In this work we state the required equations to derive a relation for the change rate of the pressure inside the chamber which consequently determines the turbine induced torque. Let us begin with a mass balance of the air chamber

$$\rho_{\text{c}_i} \dot{V}_{\text{c}_i}(t) + \dot{\rho}_{\text{c}_i} V_{\text{c}_i}(t) = -\dot{m}_{\text{t}_i}(t), \tag{8}$$

where $V_{\text{c}_i}(t)$ denotes the instantaneous chamber volume as a function of the relative position between the piston and the buoy, with the chamber air density ρ_{c_i} and $\dot{m}_{\text{t}_i}(t)$ the mass flow through the turbine, defined positive for an exhalation. Let us define the dimensionless relative pressure inside the chamber with the atmospheric pressure p_{at}, i.e.

$$p_i^*(t) = \frac{p_{\text{c}_i}(t) - p_{\text{at}}}{p_{\text{at}}} = x_{p^*,i}(t). \tag{9}$$

Considering air as a perfect gas, we can compute the air density based on the pressure difference,

$$\rho_{\text{c}_i}(t) = \rho_{\text{at}}(x_{p^*,i}(t) + 1)^{\frac{1}{\gamma}}, \tag{10}$$

with specific heat ratio $\gamma \approx 1.4$. With help of the logarithmic derivative $L(f) := \dot{f}/f$ of (10) we obtain,

$$\gamma \frac{\dot{\rho_{\text{c}_i}}(t)}{\rho_{\text{c}_i}(t)} = \frac{\dot{x}_{p^*,i}(t)}{x_{p^*,i}(t) + 1}. \tag{11}$$

Substituting the reference air density (10) and its dynamics (11) into (8) results in the time rate of change of the pressure,

$$\dot{x}_{p^*,i}(t) = -\gamma \frac{\dot{m}_{\text{t}_i}(t)}{\rho_{\text{at}} V_{\text{c}_i}(t)} \left(x_{p^*,i}(t) + 1 \right)^{\frac{\gamma-1}{\gamma}} - \gamma \frac{\dot{V}_{\text{c}_i}(t)}{V_{\text{c}_i}(t)} \left(x_{p^*,i}(t) + 1 \right). \tag{12}$$

Detailed models and experiments with the biradial turbine can be found in [12] and a suitable generator for this type of turbine is investigated in [10]. In this work we model turbine/generator set dynamics in terms of angular rotational speed with

$$\dot{\Omega}_i = \dot{x}_{\Omega,i}(t) = \frac{1}{J} \left(T_{\text{turb}_i} - T_{\text{gen}_i} - B x_{\Omega,i} \right), \tag{13}$$

where J is the composite moment of inertia (MOI) of the i^{th} turbine/generator set, B is a constant that models viscous friction losses. The instantaneous torque induced by the air pressure of the air flow through the i^{th} turbine T_{turb_i}, will be called turbine torque and T_{gen_i} denotes the instantaneous generator torques of the i^{th} WEC. The generator torque is defined to be the first control input

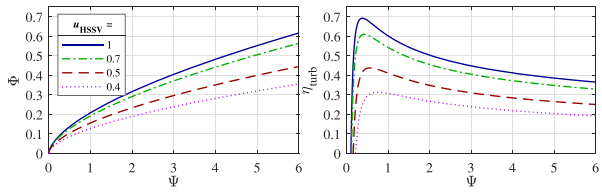

Fig. 3. Turbine characteristics as functions of the dimensionless pressure head Ψ and the position of the HSSV. Namely, efficiency η, dimensionless flow rate Φ and dimensionless power coefficient Π from [11]. Open valve: $u_{\text{HSSV}} = 1$.

$$u_{\text{gen},i} = T_{\text{gen},i}, \tag{14}$$

to our system. We do not model the detailed generator current equations assuming the generator electromagnetic dynamics are much faster than the system dynamics of the WEC and assuming the generator is run in torque mode, assuring to receive T_{gen} commanded by the drive. The turbine torque is identified with the pressure dependent dimensionless turbine performance characteristics of the turbine illustrated in Fig. 3. Those experimentally derived turbine characteristics from [11] are normalized with the rotational speed $x_{\Omega,i}$, the turbine diameter d_{turb} and the reference air density $\rho_{\text{in},i}$. Furthermore, the turbine characteristics change with the position of the HSSV, which limits the air flow into the turbine. Depending on an inhalation, or exhalation the density of the mass flow alternates as follows:

$$\rho_{\text{in}_i} = \max\left(\rho_{\text{at}}, \rho_{\text{c}_i}(t)\right). \tag{15}$$

The dimensionless pressure head which defines all other turbine characteristics and is used for the control of the HSSV can now be computed as

$$\Psi_i(x_{p^*,i}, x_{\Omega,i}) = p_{\text{at}} x_{p^*,i} / (\rho_{\text{in}_i} x_{\Omega,i}^2 d_{\text{turb}}^2), \tag{16}$$

The dimensionless mass flow rate coefficient of a turbine is defined by

$$\Phi_i(\Psi_i, u_{\text{HSSV}}) = \dot{m}_{\text{t}_i} / (\rho_{\text{in}_i} x_{\Omega,i} d_{\text{turb}}^3), \tag{17}$$

and is depending on the position of the HSSV, which is defined to be the second control input

$$u_{\text{HSSV},i} \quad \in [0, 1]. \tag{18}$$

The dimensionless power coefficient is given by

$$\Pi_i(\Psi_i, u_{\text{HSSV}}) = P_{t_i} / (\rho_{\text{in}_i} x_{\Omega,i}^3 d_{\text{turb}}^5). \tag{19}$$

The combination of the three turbine characteristic coefficients is given with the turbine efficiency as follows:

$$\eta_{\text{t}_i} = \Pi_i / (\Phi_i \Psi_i). \tag{20}$$

Finally, all necessary quantities to compute the turbine torque are known, i.e.

$$T_{\text{t}_i} = \rho_{\text{in}_i} x_{\Omega,i}^2 d_{\text{turb}}^5 \Pi_i(\Psi_i, u_{\text{HSSV}}). \tag{21}$$

C. State Space Representation

We transform the equation above to represent them in state space with variable vector (1), i.e.

$$\dot{\boldsymbol{x}} = \begin{bmatrix} \dot{\boldsymbol{x}}_z \\ \dot{\boldsymbol{x}}_v \\ \dot{\boldsymbol{x}}_{p^*} \\ \dot{\boldsymbol{x}}_\Omega \end{bmatrix} = \begin{bmatrix} \boldsymbol{x}_v \\ (\boldsymbol{M})^{-1} \cdot \boldsymbol{\mathcal{F}}(\boldsymbol{x}) \\ f_{\mathrm{p}}(\boldsymbol{x}, \boldsymbol{u}_{\mathrm{HSSV}}) \\ f_{\mathrm{k}}(\boldsymbol{x}_{p^*}, \boldsymbol{x}_\Omega, \boldsymbol{u}_{\mathrm{gen}}) \end{bmatrix} \tag{22}$$

with

$$\boldsymbol{M} = \begin{bmatrix} A^\infty_{11} & \dots & A^\infty_{1\,2N} \\ \vdots & \ddots & \vdots \\ A^\infty_{2N1} & \dots & A^\infty_{2N\,2N} \end{bmatrix} + \mathrm{diag}\left(\begin{bmatrix} m_1 \\ \vdots \\ m_{2N} \end{bmatrix} \right), \tag{23}$$

containing the added mass components A^∞_{ij} and additional on the diagonal the bodies' physical masses m_i. This matrix arises when isolating the highest derivatives on the left hand side of (2) and (3) originating from the radiation force component $F_i^{\mathrm{R},\infty}$ in (5). The matrix $(\boldsymbol{M})^{-1}$ can be regarded similar to a moment of inertia and additionally it adds hydrodynamic interactions between all bodies to the system when multiplied with the composite force, which would otherwise act on a single body, namely,

$$\boldsymbol{\mathcal{F}}(\boldsymbol{x}) = \begin{bmatrix} F_1^{\mathrm{H}}(x_{z_1}) + F_1^{\mathrm{M}}(x_{z_1}) + F_1^{\mathrm{PTO}}(x_{p_1^*}) + F_1^{\mathrm{R'}}(\boldsymbol{x}_v) + F_1^{\mathrm{Ex}} \\ \vdots \\ F_{2N}^{\mathrm{H}}(\cdot) + F_{2N}^{\mathrm{M}}(\cdot) + F_{2N}^{\mathrm{PTO}}(\cdot) + F_{2N}^{\mathrm{R'}}(\cdot) + F_{2N}^{\mathrm{Ex}} \end{bmatrix}. \tag{24}$$

III. Control Design

A. Second-Order Sliding Mode Generator Control

In our previous work [23] we present different second-order SMC controllers that are tuned for the OWC array equipped with biradial turbines and the constraint to the maximal torque. The four algorithms are derived after the fundamental work from [17]. For this work, we choose the controller with the smoothest control signal, a second-order SMC approach with a prescribed law of variance (PLV) that calculates the generator torque T_{gen} based on the rotational speed x_Ω and its time derivative $\dot{x}_\Omega$ to follow a reference angular velocity Ω_{ref}. This allows the generator to operate efficiently in terms of electric energy conversion as soon as there is a pressure difference in the air chamber. The turbine torque is considered a disturbance for the SMC algorithm, and we need to estimate the maximal expected disturbance to tune the control parameters.

1) Derivation: Starting with the entire system dynamics (22) which are rewritten as

$$\dot{\boldsymbol{x}} = \boldsymbol{f}(\boldsymbol{x}(t), u_{\mathrm{gen}}, u_{\mathrm{HSSV}}), \tag{25}$$

where $\boldsymbol{f}$ satisfies class C^1. A real generator is physically constrained to a maximal value $T_{\mathrm{gen}}^{\max}$, thus we introduce the dimensionless control input $u = u_{\mathrm{gen}}/T_{\mathrm{gen}}^{\max}$ and the SMC is designed s.t. it will keep $|u| \leq 1$. We define the sliding surface in terms of the control error between the constant reference rotational speed Ω_{ref} and the instantaneous rotational speed,

$$\boldsymbol{\sigma}(t, \boldsymbol{x}) = \Omega_{\mathrm{ref}} - \boldsymbol{x}_\Omega. \tag{26}$$

The sliding variable $\sigma(t, \boldsymbol{x})$ is of class C^2. We use the differential operator considering u constant

$$\mathcal{L}_u = \frac{\partial}{\partial t}(\cdot) + \frac{\partial}{\partial \boldsymbol{x}}(\cdot)\boldsymbol{f}(\boldsymbol{x}, \boldsymbol{u}_{\mathrm{gen}}, \boldsymbol{u}_{\mathrm{HSSV}}), \tag{27}$$

representing the total derivative with respect to (25) and define

$$\dot{\boldsymbol{\sigma}}(t, \boldsymbol{x}, u) = \mathcal{L}_u \boldsymbol{\sigma}(t, \boldsymbol{x}) = -\dot{\boldsymbol{x}}_\Omega \tag{28}$$

Now assume there exists a set $\{t, \boldsymbol{x}, u\} : |\sigma_i(t, x)| < \sigma_0$, where σ_0 is called the linearity region, such that

$$0 < K_{\mathrm{m}} < \left| \frac{\partial \dot{\sigma}_i}{\partial u} \right| < K_{\mathrm{M}}. \tag{29}$$

With the positive constants $K_{\mathrm{m}}, K_{\mathrm{M}}$. Moreover, we require the boundedness of the second derivative of the sliding surface, namely,

$$|\mathcal{L}_u \mathcal{L}_u \sigma_i(t, x)| < C_0. \tag{30}$$

If the assumptions of the bounded derivatives (29) and (30) are satisfied, the PLV algorithm [17] drives σ and $\dot{\sigma}$ towards 0 and makes the system dynamics follow the reference velocity with a smooth control input signal. This PLV algorithm computes the time rate of change of u_i, namely,

$$\dot{u}_i = \begin{cases} -u_i, & \text{if } |u_i| > c_{\mathrm{sw},i} \\ -\alpha \operatorname{sgn}(\dot{\sigma}_i - g(\sigma_i)) & \text{if } |u_i| \leq c_{\mathrm{sw},i}. \end{cases} \tag{31}$$

The choice of function $g(\sigma_i) = -\lambda \operatorname{sgn} \sigma_i |\sigma_i|^\gamma$, with $\lambda > 0$, $0.5 \leq \gamma < 1$ and

$$\alpha > \left(C_0 + \sup g'(\sigma_i) g(\sigma_i)\right) / K_{\mathrm{m}} \tag{32}$$

is a sufficient condition for convergence to the sliding surface [29]. The switching variable $c_{\mathrm{sw},i}$ limits the area of regular operation, since the control effort is opposed as soon as $|u_i| > c_{\mathrm{sw},i}$. We use $c_{\mathrm{sw},i}$ to respect the physical generator constraints and define

$$c_{\mathrm{sw},i} = \min\left(1, P_{\mathrm{rated}}^{\mathrm{gen}} / (T_{\mathrm{gen}}^{\max} x_{\Omega,i})\right), \tag{33}$$

and therefore $u_{\mathrm{gen}} \leq \min(T_{\mathrm{gen}}^{\max}, P_{\mathrm{rated}}^{\mathrm{gen}} / x_{\Omega,i})$. After time integration and scaling with the maximal generator torque the control signal for the generator is obtained,

$$u_{\mathrm{gen},i} = T_{\mathrm{gen}}^{\max} \int \dot{u}_i dt. \tag{34}$$

From our definition of the sliding surface (26) and the requirement of $\dot{\sigma}$ in the control algorithm (34) it follows that the controller needs knowledge of $\dot{x}_{\Omega,i}(t)$ in eq. (13) and therefore we need to measure the rotational speed $x_{\Omega,i}(t)$ and the relative air pressure inside the chamber $x_{p^*,i}(t)$ to use the turbine dynamics to estimate the instantaneous $T_{\mathrm{turb},i}$. In [23] we also propose an alternative that does not require $\dot{x}_\Omega$, namely a super twisting sliding mode controller from [17], but it's control signal is less smooth and it overshoots after the torque limit is reached.

2) Controller Parameters: The numerical values for the controller parameters α, λ and γ, which are based on the bounds

TABLE I
NUMERICAL SIMULATION PARAMETERS. TURBINE/GENERATOR CHARACTERISTICS FROM [12]

Quantity	sym/var	value
simulation time	T_{sim}	500 s
simulation time step	Δt	0.001 s
diameter turbine	d_{turb}	0.5 m
MOI turbine+generator	J	5.24 kg m^2
friction turbine+generator	B	0.03 N m s
reference rotational speed	Ω_{ref}	1470 rpm
nominal generator speed	$\Omega_{\text{gen}}^{\text{nom}}$	1470 rpm
maximal generator torque	$T_{\text{gen}}^{\text{max}}$	216.5 N m
rated generator power	$P_{\text{gen}}^{\text{rated}}$	30 kW
maximal generator rotational speed	$\Omega_{\text{gen}}^{\text{max}}$	3000 rpm
Lower / Upper bound first derivative σ	K_{m}; K_{M}	30.9; 51.7
Upper bound second derivative σ	C_0	150
Linearity region	σ_0	1 rad s^{-1}
slope sgn and switch approx.	c_1; c_2	50 ; 10^5
SMC parameter	α; λ; γ	6; 8; 0.5

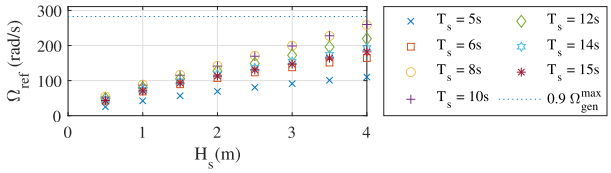

Fig. 4. Constant reference rotational speed Ω_{ref} based on the averaged rotational speed simulated with the Ideal control law.

K_{m}, K_{M} and C_0, that bound the disturbances, are given in table I and the reference rotational speed is illustrated in Fig. 4. The change rate of (28) with respect to the input is

$$\frac{\partial \dot{\sigma}}{\partial u} = \frac{T_{\text{gen}}^{\text{max}}}{J} \tag{35}$$

and we choose $K_{\text{m}} = 0.75|T_{\text{gen}}^{\text{max}}|/J$ and $K_{\text{M}} = 1.25|T_{\text{gen}}^{\text{max}}|/J$. For the second derivative we assume the density of the mass flow (10) to be constant, due to the fact that it only changes slightly when alternating for an inhalation, or an exhalation, but it simplifies the analytical derivation. Consequently,

$$\ddot{\sigma} = \mathcal{L}_u \mathcal{L}_u \sigma(t,x) \tag{36}$$

$$= \underbrace{-J^{-1}\left(\frac{\partial T_{\text{turb}}}{\partial t} + \frac{\partial T_{\text{turb}}}{\partial x_{p^*}}\dot{x}_{p^*} + \frac{\partial T_{\text{turb}}}{\partial x_\Omega}\dot{x}_\Omega - 2B\dot{x}_\Omega\right)}_{C(x,u)} + \frac{T_{\text{gen}}^{\text{max}}}{J}\dot{u}. \tag{37}$$

To identify the partial derivatives of the turbine torque, the partial derivatives of the power coefficient Π are required, which finally are a function of $\partial\Pi/\partial\Psi$, $\partial\Psi/\partial x_{p^*}$, $\partial\Psi/\partial x_\Omega$ and $\partial\Psi/\partial t$. Theoretically $C(x,u)$ is radially unbounded, however, with previous simulation of the array and knowledge of the subspace of the state space that is reached by the array of OWCs, we can numerically compute an upper bound C_0. Therefore we estimated the expected disturbance that will occur to push the system dynamics of the sliding surface. We choose $\gamma = 0.5$ and the combination $\alpha = 6$ and $\lambda = 8$ to satisfy the inequality (32). The constant reference rotational speed Ω_{ref} is based on the average rotational speed when the model is simulated with the base control law, herein it is named Ideal control law and it is described in Section III-C. This guarantees that on average there is enough energy available in the specific sea state to maintain the reference rotational speed. The resulting values are illustrated in Fig. 4 as function of the significant wave height H_{s} and the peak wave period T_{p}.

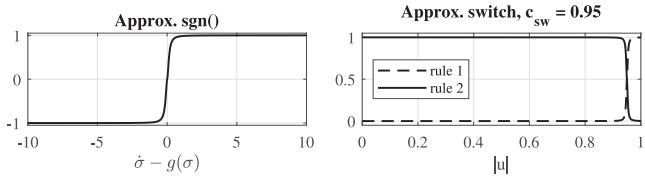

Fig. 5. Smooth functions approximating the sgn function and the switch.

3) Convergence: For the proof of convergence of the SMC PLV algorithm, the reader is referred to [17] and in more detail to [30]. The PLV algorithm steers the rotational speed trajectory into the linear region $|\sigma(x)| < \sigma_0$. The determined bounds and the accordingly chosen constant control parameters guarantee that the control law maintains the system dynamics in the neighborhood of the sliding surface. While $|u| \leq c_{\text{sw}}$ the SMC algorithm yields switching surface trajectories converging to the neighborhood of the σ-$\dot{\sigma}$ plane illustrated in our previous work [23]. When reaching the control limit, the rotational speed trajectory might leave the sliding surface. Still, the oscillating nature of the ocean waves always allows a new reaching phase to re-reach the sliding surface.

4) Practical Implementation: The nature of the higher-order SMC, i.e. that the high frequency switching action is contained in an integral function, theoretically achieves a smooth control signal already. However, for a simulation time step size in the milliseconds range the chattering in our setup is still observable. Therefore, for a more practical implementation, we approximate the sgn function and the switch when the control output exceeds the switching variable $|u_i| > c_{\text{sw}}$ with smooth functions illustrated in Fig. 5, inspired by the "sigmoid function" in [30]. The approximation entails only a "Quasi-Sliding Mode" and the steepness of the curve is chosen as trade-off between ideal performance and smoothness of the resulting signal.

B. Control for the HSSV

The main goal in controlling the position u_{HSSV} of the high-speed stop valve is to discard mechanical turbine power, once the instantaneous turbine torque gets *close* to the maximal generator torque. When closing the valve, less air flows through the turbine and consequently, less torque is generated in that instants as observed in Fig. 3. However, also a bigger pressure difference to the atmosphere builds up in the air chamber. We use the relation illustrated in Fig. 6 for this work. The graph is the result of the easiest fuzzy control logic there is. We choose this approach due to it's simplicity when defining a *close* to the maximal torque and the possibility to include more input variables in the future, without having to take the air chamber nonlinearities into account.

Now, when using a numerical solver in the simulation, an algebraic loop is created because of direct dependency of $\dot{m}_{\text{t}}$ on

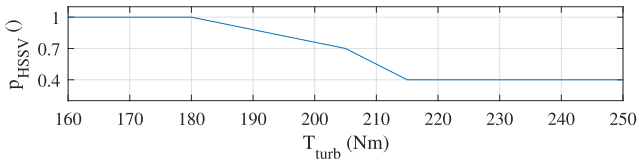

Fig. 6. Feed forward control for the position of the HSSV as a function of the instantaneous turbine torque T_{turb}.

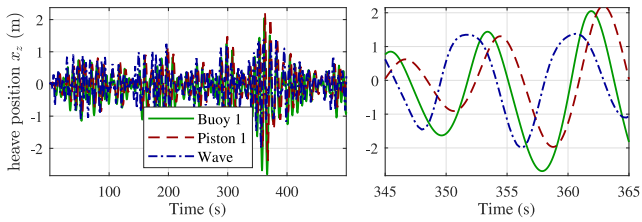

Fig. 7. WEC motion with the SMC control law.

u_{HSSV}. We avoid the algebraic loop by delaying the u_{HSSV} signal with a first-order transfer function before computing the new position of the HSSV, which further models the delay between control law and the actuation.

C. Ideal Control Law

In [9], [10] Henriques et. al. present an ideal feedback control for the generator torque based on the instantaneous angular velocity for practical use, namely,

$$u_{\text{gen},i} = \min\left(a_{\text{bep}} x_{\Omega,i}^2,\ P_{\text{gen}}^{\text{rated}}/x_{\Omega,i},\ T_{\text{gen}}^{\max}\right). \tag{38}$$

It is ideal in terms of the maximization of the aerodynamic efficiency of a fixed OWC which runs the identical biradial turbine. To determine the parameter a_{bep} at the best efficiency point, we use $\Pi(\Psi_{\text{bep}})$ and rearrange the turbine torque equation (21),

$$a_{\text{bep}} x_{\Omega,i}^2 = \underbrace{\rho_{\text{at}} d_{\text{turb}}^5 \Pi(\Psi_{\text{bep}})}_{a_{\text{bep}}} x_{\Omega}^2, \tag{39}$$

and we use the the atmospheric density as reference density. This generator control will function as a benchmark in the time domain simulation.

IV. Time Domain Simulation

We conduct the time domain simulations with MATLAB-Simulink using the fixed time step Euler (`ode1`) solver because of the solver's reliability when handling discontinuous dynamics [30]. We apply the presented control algorithms to an array of $N = 3$ WECs arranged in an equilateral triangle with 30m separation distance, with the front two WECs aligned parallel to the y-axis as in [7], [23]. We consider four cases:

1) SMC : The SMC law (34) by itself and $u_{\text{HSSV}}(t) = 1$.
2) SMC-HSSV : The SMC (34) and $u_{\text{HSSV}}(T_{\text{turb}}(t))$.
3) Ideal : The ideal control law (38) and $u_{\text{HSSV}}(t) = 1$.
4) Ideal-HSSV : The ideal law (38) and $u_{\text{HSSV}}(T_{\text{turb}}(t))$

The used simulation parameter values are listed in table I and the turbine/generator characteristics originate from [12].

A. Detailed Device Response

In [7] we show that the time evolution of the state variables of different WECs in the array are mostly shifted in time and to not to overcrowd the graphs we focus on the results of the single WEC, which is hit first when using an incident wave angle $\theta = 15°$. The results for the different control algorithms are illustrated for a wave with significant wave height $H_{\text{s}} = 2$ m and main energy period $T_{\text{p}} = 10$ s. In Fig. 7 the heave position of the incident wave, the buoy and the piston from the first WEC

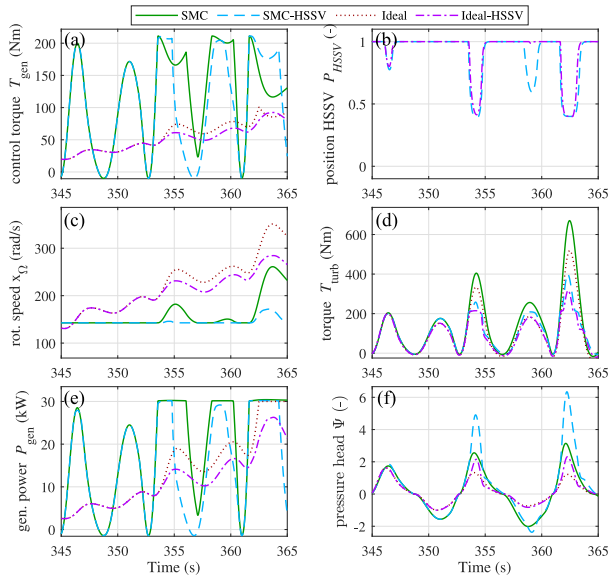

Fig. 8. Variables influencing the control algorithms. Top row: Control signals. Left column: The generator control T_{gen}, with turbine angular velocity x_Ω and electromechanical power at the generator shaft P_{gen}. Right column: The HSSV control position u_{HSSV} with turbine torque T_{turb} and dimensionless pressure head Ψ.

are illustrated for the SMC control case. The time window $T_1 \in [345, 365]$ s in the right plot is chosen to present an interval which illustrates different aspects of the control algorithms, due to temporarily phase shift of 90° between the buoy and the piston, increasing the oscillation amplitude about 110% in just two wave periods. Especially, compared to the following results as the power it has to be noted, that the difference in position between the different control cases is small with around 7% variation. Furthermore, the high relative motion results in pressure in the air chamber and consequently in turbine induced torque and good power generation potential, with the last wave oscillation resulting in a turbine torque that exceeds the maximal torque that the generator is capable to oppose.

The most relevant variables for all four control algorithms are shown in Fig. 8 with the control signals in the top row, plots a) and b). We can see from the plot c) in the middle left that the SMC (solid) follows Ω_{ref} except for three instances in time, where x_Ω leaves the sliding surface. The SMC-HSSV (dashed) leaves Ω_{ref} about 20% once in the extreme cases. Clearly, the rotational speed for the Ideal control law cases (dotted and dash-dotted) is variable and when the HSSV gets activated in the Ideal-HSSV case x_Ω decreases 8% on average over 10s, indicating that less kinetic energy is converted. To explain were the energy is going

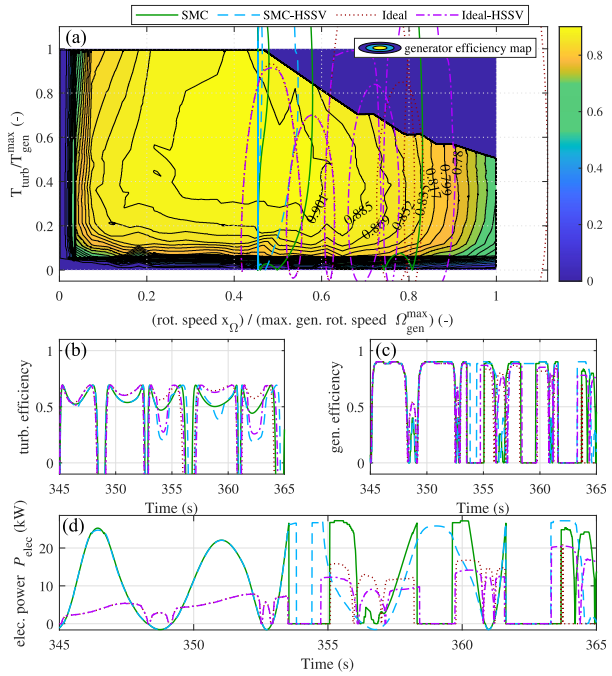

Fig. 9. Efficiency of the energy conversion and generated electric power. Left top: Efficiency map of the generator with the turbine torque over T_1 plotted into the contour. Right top: Time evolution of the turbine and generator efficiency. Bottom row: Generated electric power.

with the HSSV we take a look at the dimensionless pressure head Ψ in the Fig. 8 f) (bottom right). By closing the HSSV (illustrated in plot b), top right) a higher Ψ builds up while the buoy and piston move relatively to each other, due to the higher relative pressure inside the air chamber. However, since the HSSV limits the airflow, the resulting averaged turbine torque is 48% less for the SMC case and 34% less for the Ideal case as seen in plot d). The generator efficiency, illustrated in Fig. 9, for the electric power conversion is a function of x_Ω and T_{turb} measured at the shaft. The generator efficiency map of the implemented squirrel cage induction machine is pictured in Fig. 9 a) and originate from real measurements conducted in [11]. We plot the instantaneous turbine torque over T_1 of the cases on top of the shaded contours to comprehend the trajectories in the efficiency space.

The solid line is perfectly vertical while the constant x_Ω is achieved with the SMC. The Ideal control cases create clockwise rotating ellipsoids since x_Ω increases with T_{turb}. The extreme cases, when the efficiency map is left, occure at $t = 354$ s and $t = 363$ s. In this case the generator functions exclusively as a break and cannot convert energy anymore. Although T_{turb} exceeds the efficiency region for this short instance, T_{gen} does not exceed its maximal applicable torque as seen in Fig. 8 a) and P_{gen} stays at the rated power. The time evolution of the efficiency for the turbine and generator are given in the middle of Fig. 9, in plot c) and d) respectively. Albeit the average turbine efficiency of the SMC-HSSV over T_1 is 3% lower compared to the SMC, the electric efficiency is 20% higher, since the mechanical turbine power was discarded when the turbine torque was too high. Therefore, 13% more electric energy could be converted anyway, especially seen at $t = 359$ s in both plot c) and d). For the Ideal-HSSV case the turbine efficiency decreases approximately 5% compared to the Ideal case over the entire simulation time, but the electric generator efficiency improves by 6% with the HSSV, illustrated in Fig. 9 c). For this sea state, the SMC cases convert on average 38% more electrical power.

B. Controller Affects on Power Conversion

The effect of the SMC cases compared to Ideal case can be summarised as:

$\bar{P}_{\text{pneu}}$: The SMC/SMC-HSSV do not significantly ($\approx$0.5%) affect the averaged pneumatic power, since the motion of the buoy and the piston are not significantly altered. Hence, although the instantaneous air flow and pressure do differ, overall they balance out.

$\bar{P}_{\text{gen}}$: The SMC slightly ($<$3%) decreases the conversion from pneumatic power to turbine/generator shaft power. When using the HSSV cases $\bar{P}_{\text{gen}}$ is reduced by another 10%, because of the less efficient turbine operation with a partially closed HSSV.

$\bar{P}_{\text{elec}}$: The SMC/SMC-HSSV improves electric efficiency and electric power for low-energetic sea states because of the higher applicable generator torques that match the disturbance of the turbine torque. There is no moment of inertia that has to be overcome.

C. Averaged Array Performance

To further evaluate the power improvement capabilities in different sea states, we look at the time averaged electromechanical $\bar{P}_{\text{gen}}$ and electrical power $\bar{P}_{\text{elec}}$ beginning at 20s into the simulation, after the dynamics caused by the initial conditions settle. In Fig. 10 we present the power matrices for different combinations of T_{p} and H_{s} to represent the wave climate of Leixões, Portugal [31] for the SMC and SMC-HSSV case. We present the ratio between Ideal and SMC cases with the colors/shadings. On the left, the averaged electromechanical power is plotted and on the right, the averaged electrical power. Although the SMC law in a) does not improve the $\bar{P}_{\text{gen}}$, it improves $\bar{P}_{\text{elec}}$ by 45–65% in for the sea states with medium periods and small to medium wave heights and doubles $\bar{P}_{\text{elec}}$ for low-energetic sea states, as seen in plot b). The SMC-HSSV converted less electromechanical power than the SMC in every sea state. Nevertheless, the resulting $\bar{P}_{\text{elec}}$ is similar for the sea states around 0.5 m to 2.5 m and the SMC-HSSV performs better in the high-energetic sea states. Using the HSSV with the Ideal control law neither improves nor worsens the mechanical or the electrical power by a notable amount. However, the approach does help to reduce the very high turbine torques for the instances in time when the WEC resonates with the wave.

Although, the SMC control cases yield high improvements in multiple low-energetic sea states, when considering the annual averaged power for the wave climate in Leixões, with the frequency of occurrence of every sea state from [31], the resulting improvement is decreased. For the Ideal case the array is expected to deliver 5.56 kW averaged annual power. The SMC improves the annual power by 4.7% to 5.82 kW. With the Ideal-HSSV a 3.1% improvement is to be expected and with the SMC-HSSV the best result is achieved, with 7.9% improvement

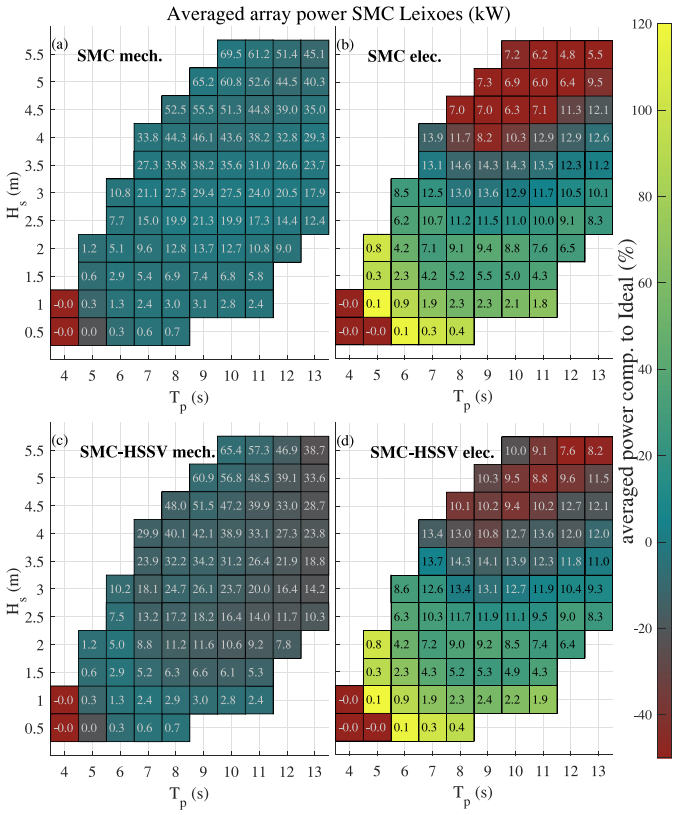

Fig. 10. Average array power for the SMC control law in the wave climate of Leixões, Portugal [31]. The color/shading indicates the comparison to the Ideal control law.

compared to the ideal case. Theoretically, if the SMC-HSSV is applied for sea states with $H_s \leq 3$ m and the Ideal-HSSV for the more energetic sea states an improvement of 19.4% compared to the Ideal case could be achieved.

Further factors to consider when choosing a controller are the power quality, the maximum rotational speed and in our case the frequency of valve operation. Based on the peak-to-average power ratio the SMC power quality is worse, with up to 30-50% higher values in most low and high-energetic sea states. However, for $H_s = 2$ m and $T_p \geq 8$ s this ratio is actually improved and with a value of 9, about 10% lower than the Ideal case. The maximal angular velocity is exceeded for some instants with the Ideal law already for $H_s \geq 2$ m and $T_p \geq 8$ s. The SMC and the SMC-HSSV could keep x_Ω below Ω_{gen}^{max} up to $H_s \geq 2.5$ m and $H_s \geq 3$ m, respectively. In the future an entire closure of the HSSV should be investigated to prevent the generator from exceeding Ω_{gen}^{max} for all cases. The HSSV is on average active for 5s more with the SMC-HSSV than with Ideal-HSSV in low sea states and vise versa in high sea states, with up to 60 activations.

V. Conclusion

The proposed control laws noticeably improve the electric power conversion of the OWC WEC array for multiple low to medium energetic sea states. By maintaining a constant reference rotational speed, appropriate for each sea state, the turbine and generator are kept in a highly efficient area of operation as soon as the air pressure accelerates the turbine. Future investigations could include a time-varying reference rotational speed resulting from an optimization problem inspired by a maximal power point tracking algorithm. However, to keep the turbine generator set at one constant speed might be interesting in the future if larger turbines, with a higher moment of inertia are deployed.

V. Disclaimer

All the data used to develop the models used in this work is publicly available [28] and the authors are not affiliated with the developers of the IDOM Marmok A-5.

References

[1] J. Falnes, *Ocean Waves and Oscillating Systems: Linear Interactions Including Wave-Energy Extraction*. Cambridge, U.K.: Cambridge Univ. Press, 2002.

[2] T. Sabuncu and S. Calisal, "Hydrodynamic coefficients for vertical circular cylinders at finite depth," *Ocean Eng.*, vol. 8, no. 1, pp. 25–63, 1981.

[3] A. F. O. Falcão, "Wave energy utilization: A review of the technologies," *Renew. Sustain. Energy Rev.*, vol. 14, no. 3, pp. 899–918, 2010.

[4] J. Andrews and N. Jelley, *Energy Science: Principles, Technologies, and Impacts*, 3rd ed. Oxford, U.K.: Oxford Univ. Press, 2017.

[5] L. Wang, J. Isberg, and E. Tedeschi, "Review of control strategies for wave energy conversion systems and their validation: The wave-to-wire approach," *Renew. Sustain. Energy Rev.*, vol. 81, pp. 366–379, 2018.

[6] S. Chowdury, *et al.*, "A review of hydrodynamic investigations into arrays of ocean wave energy converters," 2015, *arXiv:1508.00866*.

[7] D. T. Gaebele, M. E. Magaña, T. K. A. Brekken, and O. Sawodny, "State space model of an array of oscillating water column wave energy converters with inter-body hydrodynamic coupling," *Ocean Eng.*, vol. 195, p. 106668, 2020.

[8] A. F. O. Falcão and J. C. C. Henriques, "Oscillating-water-column wave energy converters and air turbines: A review," *Renew. Energy*, vol. 85, pp. 1391–1424, 2016.

[9] J. C. C. Henriques, W. Sheng, A. F. O. Falcão, and L. M. C. Gato, "A comparison of biradial and wells air turbines on the Mutriku breakwater OWC wave power plant," in *Proc. ASME 36th Int. Conf. Ocean, Offshore Arctic Eng. Volume 10: Ocean Renew. Energy*, Jun. 2017, pp. 1–12, OMAE2017-62651, V010T09A037.

[10] J. C. C. Henriques, J. C. C. Portillo, W. Sheng, L. M. C. Gato, and A. F. O. Falcão, "Dynamics and control of air turbines in oscillating-water-column wave energy converters: Analyses and case study," *Renew. Sustain. Energy Rev.*, vol. 112, pp. 571–589, Jun. 2019.

[11] A. A. D. Carrelhas, "Experimental study of the model and the prototype of a self-rectifying biradial air turbine with fixed guide-vanes. (in Portuguese)," Master Thesis, Instituto Superior Técnico, Universidade de Lisboa, 2017.

[12] A. A. D. Carrelhas, L. M. C. Gato, J. C. C. Henriques, A. F. O. Falcão, and J. Varandas, "Test results of a 30 kW self-rectifying biradial air turbine-generator prototype," *Renew. Sustain. Energy Rev.*, vol. 109, pp. 187–198, 2019.

[13] V. I. Utkin, "Sliding modes in control and optimization," in *Communication Control Engineering Ser.*, Berlin, Germany: Springer Science & Business Media, 1992.

[14] A. J. Garrido, I. Garrido, M. Alberdi, M. Amundarain, O. Barambones, and J. A. Romero, "Robust control of oscillating water column (OWC) devices: Power generation improvement," in *Proc. OCEANS - San Diego*, 2013, pp. 1–4.

[15] O. Barambones and J. G. de Durana, "Sliding mode control for power output maximization in a wave energy systems," *Energy Procedia*, vol. 75, pp. 265–270, 2015.

[16] M. E. Magaña, D. R. Brown, D. T. Gaebele, J. C. C. Henriques, and T. K. A. Brekken, "Sliding mode control of an array of three oscillating water column wave energy converters to optimize electrical power generation," in *Proc. Eur. Wave Tidal Energy Conf. Ser.*, 2019, pp. 1–10.

[17] A. Levant, "Sliding order and sliding accuracy in sliding mode control," *Int. J. Control*, vol. 58, no. 6, pp. 1247–1263, 1993.

[18] B. Beltran, M. E. H. Benbouzid, and T. Ahmed-Ali, "Second-order sliding mode control of a doubly fed induction generator driven wind turbine," *IEEE Trans. Energy Convers.*, vol. 27, no. 2, pp. 261–269, Jun. 2012.

[19] B. Meghni, D. Dib, and A. Azar, "A second-order sliding mode and fuzzy logic control to optimal energy management in wind turbine with battery storage," *Neural Comput. Appl.*, vol. 28, pp. 1417–1434, 2016.
[20] S. E. Ben Elghali, M. E. H. Benbouzid, T. Ahmed-Ali, and J. F. Charpentier, "High-order sliding mode control of a marine current turbine driven doubly-fed induction generator," *IEEE J. Ocean. Eng.*, vol. 35, no. 2, pp. 402–411, Apr. 2010.
[21] H. Chen, S. Tang, J. Han, N. AÏt-Ahmed, and T. Tang, "Second-order sliding mode current control of doubly salient permanent magnet generator," in *Proc. IECON 2019 45th Annu. Conf. IEEE Ind. Electron. Soc.*, vol. 1, 2019, pp. 7010–7015.
[22] R. Suchithra, K. Ezhilsabareesh, and A. Samad, "Optimization based higher order sliding mode controller for efficiency improvement of a wave energy converter," *Energy*, vol. 187, p. 116111, 2019.
[23] D. T. Gaebele, M. E. Magaña, T. K. A. Brekken, and J. C. C. Henriques, "Constrained sliding mode control for oscillating water column wave energy converters," in *Proc. 21st IFAC World Congr.* Berlin, Germany, Jul. 2020, pp. 12506–12512.
[24] S. V. Emelyanov and S. K. Korovin, "Applying the principle of control by deviation to extend the set of possible feedback types," in *Proc. Sov. Phys. Dokl.*, 1981, vol. 26, pp. 562–564.
[25] A. Burgaç and H. Yavuz, "Fuzzy logic based hybrid control implementation of a heaving wave energy converter," *Energy*, vol. 170, pp. 1202–1214, 2019.
[26] W. Pedrycz, *Fuzzy Control and Fuzzy Systems* (2nd, Extended Ed.). GBR: Research Studies Press Ltd., 1993.
[27] J. Lekube, A. Garrido, I. Garrido, E. Otaola, and J. Maseda, "Flow control in Wells turbines for harnessing maximum wave power," *Sensors (Basel)*, vol. 18, no. 2, p. 535, 2018.
[28] P. Etxaniz, "Wave energy: An industry with a bright future," in *Bilbao Mar. Energy Week*, Apr. 2017. Accessed: Sep. 2020. [Online]. Available: https://www.bilbaomarinenergy.com/CMSPages/GetFile.aspx?guid=a8db6a1f-3 4f4-4548-a4e7-7f4dba46a76f
[29] K. D. Young, M. Thoma, and U. Ozguener, *Variable Structure Systems, Sliding Mode and Nonlinear Control*, 1st ed. Berlin, Heidelberg: Springer-Verlag, 1999.
[30] Y. Shtessel, C. Edwards, L. Fridman, and A. Levant, *Sliding Mode Control and Observation*. New York, NY, USA: Springer-Verlag, 2014.
[31] J. C. C. Portillo *et al.*, "Wave energy converter physical model design and testing: The case of floating oscillating-water-columns," *Appl. Energy*, vol. 278, p. 115638, 2020.

Daniel T. Gaebele (Student Member, IEEE) received the B.S. and M.S. degrees in engineering cybernetics from the University of Stuttgart, Germany, in 2015 and 2018, respectively. After interning in a German start-up with first commercial WEC projects in 2018, he joined the School of Electrical Engineering and Computer Science at Oregon State University to working toward the Ph.D in electrical engineering with research focus on modeling and control of wave energy converter parks.

Mario E. Magaña (Senior Member, IEEE) received the B.S. degree from Iowa State University, in 1979, the M.S. degree from the Georgia Institute of Technology, in 1980, and the Ph.D. degree also from Purdue University, in 1987, all in electrical engineering. He is currently an Associate Professor with Electrical Engineering, Oregon State University, Corvallis, OR. He was a Fulbright Professor with the National University of La Plata, Argentina and was an Invited Researcher/Lecturer, the Universities of Ulm, Stuttgart, and Offenburg in Germany, and with the Technical University of Catalunya in Barcelona, Spain. Prior to joining the Faculty at Oregon State University, he spent several years working with the Analysis and Technology Group of the Communications Systems Division with the Harris Corporation in Melbourne, FL, in the Flight Control Systems Research Unit at the Boeing Company in Seattle, WA, and at NASAs Marshall Space Flight Center in Huntsville, AL. He is the Author of more than 100 technical and scientific papers, and has written two books on network coding and one on structural control. His current areas of research include the fields of mobile wireless communications and automatic control applications.

Ted K. A. Brekken (Senior Member, IEEE) received the B.S., M.S., and Ph.D. degrees from the University of Minnesota in 1999, 2002, and 2005 respectively. He is a Professor in Energy Systems with Oregon State University. He studied wind turbine control with the Norwegian University of Science and Technology in Trondheim, Norway in 2004–2005 on a Fulbright scholarship. He is Co-Director of the Wallace Energy Systems and Renewables Facility. His research interests include control and modeling of renewable energy systems and electrical system resilience. He was the recipient of the NSF CAREER award, the IEEE Power and Energy Outstanding Young Engineer award, and numerous teaching awards.

João C. C. Henriques was born in Lisbon, Portugal, in 1969. He received the Diploma, M.Sc., and the Ph.D. degrees in mechanical engineering from the Instituto Superior Técnico (IST), Technical University of Lisbon (presently University of Lisbon), in 1993, 1996, and 2006, respectively. He has authored or coauthored 50 papers in peer-refereed journals. He also holds five patents, four in the field of wave energy and another in wind power. From 1993 to 2007, his main research topic was the development of numerical methods for simulating high-speed compressible flow. His research interests include numerical and experimental modeling of wave energy converters (WECs), control of the power take-off system of WECs and the aerodynamic design of air turbines for oscillating water column WECs. He participated in eight European projects in the area of wave energy. Presently is an Assistant Professor with IST and a member of Instituto de Engenharia Mecânica (IDMEC).

Ana A. D. Carrelhas received the M.Eng. degree in mechanical engineering with specialization in energy system from Instituto Superior Técnico, Lisbon, Portugal. Her master's thesis received an award by the renowned institution EUREC. She is currently working toward the Ph.D. degree in sustainable energy systems by MIT-Portugal. Her R&D experience comprises experimental work in laboratories and wave tanks, fieldwork (onshore and offshore) and numerical modeling.

Luís M. C. Gato received the first degree (5-year course) from IST, UL, in 1979 and the Ph.D. degree from IST, UL, in 1989, both in mechanical engineering. He is an Associate Professor in Mechanical Engineering with Instituto Superior Técnico (IST), Universidade de Lisboa (UL). His main research interests include wave energy conversion (especially of oscillating water column type), power take-off equipment for wave energy converters and turbomachinery. He is a member of Instituto de Engenharia Mecânica (IDMEC), a research centre affiliated with IST. He is the Coordinator of the Specialisation Semester in Ocean Energy of the EUREC M.Sc. degree in Renewable Energy with IST. He has supervised or Co-Supervised ten Ph.D. theses. Participated, or is currently involved, in more than 30 international research projects and 15 national research projects, funded by public entities and the industry. He has authored or coauthored more than 70 papers in international peer-reviewed journals. He also holds five patents in the field of wave energy. He is Member of the Steering Committee of the Implementing Agreement on Ocean Energy Systems, International Energy Agency.